Available online at www.rajournals.in

RA JOURNAL OF APPLIED RESEARCH
ISSN: 2394-6709
DOI:10.47191/rajar/v10i07.01
Volume: 10 Issue: 07 July-2024

International Open Access

Impact Factor- 8.174

Page no.- 129-140

A High Temperature Lithium-Oxygen/Air Fuel Cell Formulation

Sarwan S. Sandhu[1*], Kevin Hinkle[2], Joseph P. Fellner[3]
[1,2]Department of Chemical and Materials Engineering, University of Dayton, Dayton, OH 45469, USA
[3]Air Force Research Laboratory, Wright-Patterson AFB, OH 45433, USA

ARTICLE INFO

Published Online:
06 July 2024

Corresponding Author:
Sarwan S. Sandhu

ABSTRACT

The formulation presented in this paper has been developed for the design and performance analysis of a high temperature lithium/oxygen or air fuel cell. The formulation predicts the cell open-circuit voltage (EMF), thermodynamic efficiency; the lithium (fuel) fractional conversion and formation of the solid product (di-lithium monoxide) as a function of the cell operational time; the net cell-mass increase rate at a constant cell current; and the ratio of (the net cell-mass increase rate) to (its electric power delivery to an external electric load) as a function of the cell temperature.

The numerical data calculated from the formulation predicts a decrease in the cell open-circuit voltage with an increase in the cell temperature. The cell open-circuit voltage is larger at 5bar than that at 1bar with air being the cell oxidant source over the temperature range of 298.15-1100 K. The cell ideal thermodynamic efficiency decreases with an increase in the cell operational temperature from about 94 to 77% over the temperature range mentioned above. Also, the ratio of [(the net cell-mass increase rate) to (the cell electric power delivery to an external electric load)] increases with an increase in the cell operational temperature. Finally, it is recommended that a physical system of the type sketched in Figure 1 be built for the acquisition of the open-circuit cell voltage as well as the operational cell voltage data for the constant cell current levels at the isothermal and isobaric conditions to validate the predictions of the presented formulation.

1. INTRODUCTION

The work reported in this relatively short paper is in connection with our pursuit to develop the electrochemical systems, fuel cells and batteries [1-27] to deliver the electric power more efficiently and safely for the space and terrestrial applications. The formulation for the high temperature fuel cell sketched in Figure 1 has been developed for its design and performance analysis.

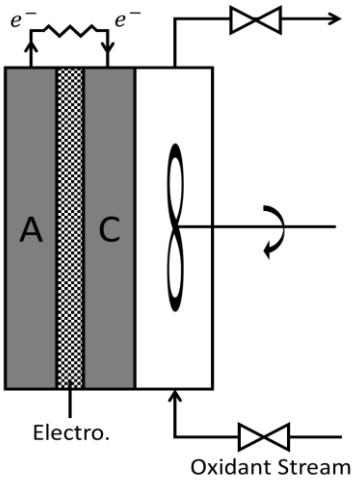

Figure 1. High temperature lithium-oxygen/air fuel cell.

The major components of the fuel cell shown in Fig. 1 are

C (cathode)- Porous strontia-doped lanthanum manganite perovskite, $La_{1-x}Sr_xMnO_3$; $0.1< x <0.15$ [28]. The cell cathode-side reactant is oxygen.

Electro (electrolyte)- Solid solution of scandia-in-zirconia, $(ZrO_2)_{1-x}(Sc_2O_3)_x$; with x = 0.1 or 10 mol% of Sc_2O_3 in the mixture with zirconia as the solvent. It has the ionic conductivity:

$0.03\text{-}0.19\ \left(S.cm^{-1}=(ohm\text{-}cm)^{-1}\right)$ over the temperature range of 973-1173 K (i.e. 700-900°C[29]).

A (anode): Thin lithium-aluminum alloy layer in contact with the electrolyte. The cell anode-side reactant is lithium.

The developed formulation is provided in Section 2. The data computed from the formulation is presented in Section 3 which is followed by Section 4- discussion of the computed data. Section 5 summarizes 'some concluding remarks.'

2. FORMULATION

The overall cell reaction is

$$2Li+\frac{1}{2}O_2(g)\rightarrow Li_2O(cr) \qquad (1)$$

At a cell temperature T[K], the standard-state Gibbs free energy change of the cell reaction, Eq. (1) is given [31] by

$$\Delta G^o_T=\Delta G^o_{T_0}\left(\frac{T}{T_0}\right)+\Delta H^o_{T_0}\left(1-\frac{T}{T_0}\right)+\frac{1}{T}\int_{T_0}^{T}\Delta C^o_p dT-\int_{T_0}^{T}\left(\frac{\Delta C^o_p}{T}\right)dT, \qquad (2)$$

where $\Delta G^o_{T_0}$ and $\Delta H^\circ_{T_0}$ are, for the reaction, Eq. (1), the Gibbs free energy change and enthalpy change at the reference temperatutre, T_0 = 298.15K; with the chemical species involved in the reaction in their respective standard states.

$\Delta C^o_p=\left(C^o_{p,Li_2O(cr)}-\left(2C^{\circ}_{p,Li}+\frac{1}{2}C^o_{p,O_2(g)}\right)\right)$, the standard-state heat capacity change associated with the reaction, Eq. (1).

$\Delta G^o_{T_0}$ and $\Delta H^o_{T_0}$ are given by

$$\Delta G^o_{T_0}=\left[G^o_{Li_2O(cr),T_0}-\left(2G^o_{Li,T_0}+\frac{1}{2}G^o_{O_2(g),T_0}\right)\right],\ \left(J.mol^{-1}\text{of the reaction, Eq. (1)}\right) \qquad (3\text{-a})$$

$$=\left[\Delta G^o_{f,Li_2O(cr)}-\left(2\Delta G^o_{f,Li,T_0}+\frac{1}{2}\Delta G^o_{f,O_2(g),T_0}\right)\right] \qquad (3\text{-b})$$

With $\Delta G^o_{f,Li,T_0}=\Delta G^o_{f,O_{2(g),T_0}}=0.0\ (J.mol^{-1})$ for the elemental species, Eq. (3-b) reduces to:

$$\Delta G^o_{T_0}=\Delta G^o_{f,Li_2O(cr),T_0}=\left(-562.102\times10^3\right)J.mol^{-1} \qquad (4)$$

Also, $\Delta H^o_{T_0}=\left[H^o_{Li_2O(cr),T_0}-\left(2H^o_{Li(cr),T_0}+\frac{1}{2}H^o_{O_2(g),T_0}\right)\right],\left(J.mol^{-1}\right)$ of the reaction, Eq. (1). (5)

$$=\left[\Delta H^o_{f,Li_2O(cr),T_0}-\left(2\Delta H^o_{f,Li(cr),T_0}+\frac{1}{2}\Delta H^o_{O_2(g),T_0}\right)\right] \qquad (5\text{-a})$$

With $\Delta H^o_{f,Li(cr),T_0}=\Delta H^o_{O_2(g),T_0}=0.0$, $\left(J.mol^{-1}\right)$ for the elemental species; Eq. (5-a) reduces to:

$$\Delta H^o_{T_0}=\Delta H^o_{f,Li_2O(cr),T_0}=\left(-598.730\times10^3\right),\left(J.mol^{-1}\right). \qquad (5\text{-b})$$

In the determination of ΔG_T^o, Eq. (2), the effect of the terms invoving ΔC_p^o is very small (for example, of the order of 0.2% or less) relative to the first two terms.

Therefore, Eq. (2) is reduced to

$$\Delta G_T^o = \Delta G_{T_0}^o \left(\frac{T}{T_0}\right) + \Delta H_{T_0}^o \left(1-\frac{T}{T_0}\right), \left(\text{J.mol}^{-1}\text{of the reaction, Eq. (2)}\right). \qquad (6)$$

The standard-state cell voltage at a temperature, T[K], is given by

$$E_T^o = \left(\frac{-\Delta G_T^o}{nF}\right), \left(\text{J.mol}^{-1}\text{of the reaction, Eq. (1)}\right), \qquad (7)$$

where n = g-equivalents of the reaction, Eq. (1) occurring, F = Faraday's constant = 96487.00 coulombs per g-equivalent. For the reaction, Eq.(1), n = 2.

The actual cell open-circuit voltage for the reaction, Eq. (1), is given by the following Nerst-type equation:

$$E_T = E_T^o - \left(\frac{RT}{nF}\right) \ln\left(\frac{a_{Li_2O(cr)}}{a_{Li(cr)}\left(\hat{a}_{O_2(g)}\right)^{\frac{1}{2}}}\right) \qquad (8)$$

where a_i = activity of a pure chemical species i, $\hat{a}_i$ =activity of a species in a mixture, and R = the universal gas constant = 8.314 $\text{J.mol}^{-1}.\text{K}^{-1}$.

Here, $a_{Li(cr)} = a_{Li_2O(cr)} = 1$. For the oxygen supply to the cell from the dry air feed, the oxygen activity is given by

$$\hat{a}_{O_2(g)} = \frac{\hat{f}_{O_2(g)} p_{O_2(g)}}{P^o} = \frac{\hat{f}_{O_2(g)} y_{O_2(g)} P}{P^o} \qquad [31], \qquad (9)$$

$\phi_{O_2(g)} = \phi_{O_2(g)}\{T, P, y_j\} =$ fugacity coefficient of oxygen to account for its nonideal gas behavior; especially, when the air feed pressure is greater than 5 bar. Otherwise, it can be assumed to be equal to 1. Then, for P < 5 bar,

$$\hat{a}_{O_2(g)} = \frac{y_{O_2(g)} P}{P^o} \ , \qquad (10)$$

where $y_{O_2(g)}$ = oxygen mole fraction in the cell cathode-side dry air feed channel, P = total pressure in the air feed channel (bar) and P° = standard pressure = 1bar.

By the use of the above given technical information, Eq. (8) is reduced to

$$E_T = E_T^o - \left(\frac{RT}{2F}\right) \ln\left[\frac{1}{\left(\frac{y_{O_2(g)} P}{P^o}\right)^{\frac{1}{2}}}\right] \text{(volt)} \qquad (11)$$

Simplification of Eq. (11) leads to

$$E_T = E_T^o + \left(\frac{RT}{4F}\right)\left[\ln(y_{O_2(g)}) + \ln\left(\frac{P}{P^o}\right)\right] \ , \text{(volt)} \ . \qquad (12)$$

If the fuel cell is delivering electric power to an 'external' electric load at a certain current level, $I^{cell}(\text{amp})$; then, the actual cell voltage is given by

$$E_{actual}^{cell} = \left[E_T - \left(\left|\eta^C\right| + \left|\eta^A\right| + \left|\eta^{ohm}\right| + \left|\eta^{conc}\right| \right) \right], \text{ (volt) .} \qquad (13)$$

$$\left(\begin{array}{l} \text{valid in the absence of cross-over of reactant species through the cell electrolyte} \\ \text{from one electrode to the other electrode of the fuel cell} \end{array} \right)$$

In Eq. (13), $\left|\eta^C\right|$ and $\left|\eta^A\right|$ = magnitude of the activation polarization voltage loss associated with the electrochemical reaction occurring on the active sites of the electro-active surface of the cell cathode and anode, respectvely. $\left|\eta^{ohm}\right|$ = ohmic voltage loss due to the resistance to ion transport $\left(\text{e.g. } O^{=} \text{ transport}\right)$ through the cell electrolyte and cathode electrode, and the resistance to electron migration through the cell electrodes plus the cell terminal resistance. $\left|\eta^{conc}\right|$ = magnitude of the cell concentration polarization or voltage loss due to lower concentrations of the cell reactant species at the cell electrode electro-active surfaces. The reactant species concentrations at the electrode electrochemical-reaction active surfaces are not maintained; especially, at high cell current levels. Transport of the charge neutral species takes place via the diffusion process or (diffusion coupled with induced convection). Electrochemical reaction activity at the active surface of a cell electrode would decrease due to the existence of the spatial gradients of the concentrations of the chemical species involved in an electrode reaction. Also, the accumulation of the reaction product species over the active sites of a cell electrode surface would cause a decrease in its electrochemical reaction rate per unit active surface area. But to maintain the same total cell current, this would result in additional voltage loss.

Thermodynamic efficiencies of a fuel cell, here, defined as follows:

$$\eta_T^o = \frac{\Delta G_T^o}{\Delta H_T^o} \qquad (14)$$

$$\eta_T = \frac{\left(-nFE_T\right)}{\Delta H_T^o} \qquad (15\text{-a})$$

$$= \frac{\left(-2FE_T\right)}{\Delta H_T^o}, \text{ for } n = 2. \qquad (15\text{-b})$$

For the cell operating at the actual isothermal, steady-state conditions; delivering electric power to an 'external' electric load at a cell current of I^{cell} (amp); the measured or predicted cell voltage is represented as E_{actual}^{cell}, (volt). The actual cell thermal efficiency is given by

$$\eta_T^{actual} = \frac{\left(-nFE_{actual}^{cell}\right)}{\Delta H_T^o} \qquad (16\text{-a})$$

$$= \frac{\left(-2FE_{actual}^{cell}\right)}{\Delta H_T^o}, \left(\text{for } n = 2, \text{ for the cell reaction, Eq. (1)}\right) \qquad (16\text{-b})$$

It is likely that E_{actual}^{cell} would decrease as a function of time for the cell operation at a constant current level; then, η_T^{actual} would be indicative of the instantaneous thermodynamic efficiency of the operating cell.

Formulation for the determination of the increase in the cell mass as a function of the cell operational time excluding the molecular oxygen mass:

Say, the initial amount of lithium (fuel) in the cell = $N_{Li,0}$ moles (in fact, g-atoms). (17)

At the time, t (sec) in the cell operation, amount of lithium = N_{Li} moles. (18)

The lithium fractional conversion during the time period, t(sec), is defined as

$$X_{Li} = \frac{N_{Li,0} - N_{Li}}{N_{Li,0}} = 1 - \frac{N_{Li}}{N_{Li,0}} \quad (19)$$

Therefore, $N_{Li} = N_{Li,0}\left(1 - X_{Li}\right)$ moles = [lithium amount still available at time t(sec) for its conversion].

(20)

According to the cell overall reaction, Eq. (1); at time t(sec), the rate of change in the amount of lithium in the cell delivering electric power at a cell current level of I(amp) is given by

$$-\frac{dN_{Li}}{dt} = \frac{I^{cell}}{F} \left(mol.s^{-1}\right) \quad (21)$$

By the combination of Eq. (20) and (21), the following relation is obtained:

$$\frac{dX_{Li}}{dt} = \frac{I^{cell}}{FN_{Li,0}}, \left(s^{-1}\right). \quad (22)$$

Molar production rate of dilithium monoxide, $Li_2O(cr)$, $\dot{N}_{Li_2O(cr)} = \frac{I^{cell}}{2F}, \left(\text{moles of } Li_2O(cr).s^{-1}\right)$.

(23)

Integration of Eq. (21) and (22), and further simplification leads to:

$$N_{Li} = N_{Li,0} - \frac{1}{F}\left(\int_0^t I^{cell} dt\right), \left(\text{moles}\right). \quad (24)$$

$$X_{Li} = \frac{1}{FN_{Li,0}} \int_0^t I^{cell} dt, \ (\text{dimensionless}). \quad (25)$$

For the constant-current cell operation; Eq. (24) and (25), respectively, becomes

$$N_{Li} = N_{Li,0} - \frac{I^{cell} t}{F}, (\text{moles}). \quad (26)$$

$$X_{Li} = \frac{I^{cell} t}{FN_{Li,0}}, \ (\text{dimensionless}). \quad (27)$$

Integration of Eq. (23) with respect to time leads to:

$$N_{Li_2O(cr)} = N_{Li_2O(cr),0} + \frac{\int_0^t I^{cell} dt}{2F}, \quad (\text{moles}). \quad (28)$$

For the constant-current cell operation, Eq. (28) becomes

$$N_{Li_2O(cr)} = N_{Li_2O(cr),0} + \frac{I^{cell} t}{2F}, \ (\text{moles}). \quad (29)$$

where $N_{Li_2O(cr),0} = \left(\text{initial moles of } Li_2O(cr) \text{ at } t = 0.0 \text{ sec.}\right)$.

If $N_{Li_2O(cr)} = 0.0$ (mole) ;then, Eq. (29) reduces to:

$$N_{Li_2O(cr)} = \left(\text{moles of dilithium monoxide(cr) in the cell at time, t(sec), in the cell operation}\right)$$

$$= \frac{I^{cell} t}{2F} \ (\text{moles}) = \left(\text{amount of } Li_2O(cr) \text{produced via the cell reaction, Eq. (1)}\right).$$

(30)

At time, t (sec), of the cell operation to deliver electric power to an external load at a constant current, I^{cell} (amp), the total amount of (lithium+ $Li_2O(cr)$) is given by

$$N_{Li+Li_2O(cr)} = \left(N_{Li,0} - \frac{I^{cell}t}{F} \right) + \left(\frac{I^{cell}t}{2F} \right) = \left(N_{Li,0} - \frac{I^{cell}t}{2F} \right), \text{(moles)}. \quad (31)$$

The total mass of (lithium + dilithium monoxide, $Li_2O(cr)$) at time, t (sec), in the cell operation, is

$$m_{(Li+Li_2O(cr))} = \left[\left(N_{Li,0} - \frac{I^{cell}t}{F} \right) M_{Li} \right] + \left[\left(\frac{I^{cell}t}{2F} \right) M_{Li_2O} \right], \text{(gm)}, \quad (32)$$

where, M_{Li} = atomic weight of lithium = 6.941 $gm.mol^{-1}$, M_{Li_2O} = molecular weight of dilithium monoxide = 29.88 $gm.mol^{-1}$.

Simplification of Eq. (32) leads to:

$$m_{(Li+Li_2O(cr))} = \left(N_{Li,0} M_{Li} \right) + \left(\frac{I^{cell}t}{F} \right) \left(\frac{M_{Li_2O}}{2} - M_{Li} \right), \text{(gm)}. \quad (33)$$

Or

$$m_{(Li+Li_2O(cr))} = \left[6.941 N_{Li,0} + 7.999 \left(\frac{I^{cell}t}{F} \right) \right], \text{(gm)}, \quad (34)$$

where $N_{Li,0} = (\text{initial g-atoms of lithium charged to the cell})$. It is here noted that the numerical number (7.999 in Eq. (34)) is effectively equal to the mass of the oxygen reactant consumed to a gram-mole of the solid dilithium monoxide.

For the cell operation at a constant current level of $I(amp)$, the rate of change of the total mass of $(Li + Li_2O(cr))$ is given as

$$\dot{m}_{(Li+Li_2O(cr))} = \frac{dm_{(Li+Li_{2O}(cr))}}{dt} = (\text{rate of net increase of cell mass}) = \left(7.999 \left(\frac{I^{cell}}{F} \right) \right), (gm.s^{-1})$$

$$= \left(7.999 \times 10^{-3} \left(\frac{I^{cell}}{F} \right) \right), \left(kg.s^{-1} \right). \quad (35)$$

At the cell operational time of t (sec); if the actual cell voltage is $E_{actual}(volt)$, then the actual cell power delivery to an external load is given by

$$\dot{P} = \left(I^{cell} E_{actual} \right), (W). \quad (36)$$

At any time during the period of the cell operation, the ratio of the cell net mass increase rate to its electric power delivery is given as

$$\left[\frac{\dot{m}}{\dot{P}} \right] = \left[\frac{7.999}{FE_{actual}} \right], \left(\frac{kg.s^{-1}}{kW} \right) = \left[\frac{8.2902 \times 10^{-5}}{E_{actual}} \right], \left(\frac{kg.s^{-1}}{kW} \right) = \left[\frac{0.2984}{E_{actual}} \right], \left(\frac{kg.hr^{-1}}{kW} \right), \quad (37)$$

where $E_{actual} = (\text{actual cell voltage at time, t (sec), during the period of the cell operation}), (volt)$.

For the situation of negligible total cell voltage loss associated with the polarizations of the electrode electrochemical reactions and the transport of the species; e.g. ions, electrons and oxygen; in the various cell components; especially, at a low cell current level, Eq. (37) becomes

$$\left[\frac{\dot{m}}{\dot{P}} \right] = \left[\frac{0.2984}{E_T} \right], \left(\frac{kg.hr^{-1}}{kW} \right). \quad (38)$$

The cell e.m.f. E_T is given by Eq, (12). Notice, the larger the E_{actual} or E_T, the smaller the ratio

$\left[\frac{\dot{m}}{\dot{P}}\right]$.

Initial weight of lithium, $m_{Li,0} = \left(N_{Li,0}M_{Li}\right) = \left(6.941N_{Li,0}\right)$, (gm). (39)

From Eq. (35 and (39), the following equation is obtained,

$$\left[\frac{\dot{m}_{(Li+Li_2O(cr))}}{m_{Li,0}}\right] = \left(\frac{1.1944\times10^{-5}I^{cell}}{N_{Li,0}}\right), (s^{-1}), \quad (40)$$

where $N_{Li,0}$ = (initial g-moles (in fact, g-atoms) of lithium charged to the cell).

For the cell operational conditions; especially, at a low cell current level; when $\eta^A = \eta^C = \eta^{conc} = 0.0$ (volt), Eq. 13) results in

$$E_{actual} = E_T - \left|\eta^{ohm}\right|, (volt). \quad (41)$$

With the assumption of negligible ohmic-type resistance to the transport of ions and electrons in the cell electrodes as well as of negligible contact resistance to electron transport at the cell terminals, Eq. (41) becomes

$$E_{actual} = E_T - \left|\eta^{ohm}_{electrolyte\text{-}separator}\right|, (volt). \quad (42)$$

$$\left|\eta^{ohm}_{electrolyte\text{-}seaparator}\right| = \left[\frac{i_{geom}\times l_{electrolyte\text{-}separator}}{\sigma_T}\right], (volt). \quad (43)$$

Where, $i_{geom} = \left(\text{cell geometric current density, in amp. } cm^{-2}_{geom}\right)$; $l_{electrolyte\text{-}separator} = \left(\begin{array}{l}\text{thickness of the}\\ \text{electrolyte-separator,}\\ \text{in cm}\end{array}\right)$;

$\sigma_T = \left(\text{ionic conductivity of the electrolyte in the separator, } S.cm^{-1}, \text{ at the cell temperature, } T[K]\right)$.

Combining Eq. (42) and (43),

$$E_{actual} = \left(E_T - \left(\frac{i_{geom}l_{electrolyte\text{-}separator}}{\sigma_T}\right)\right), (volt). \quad (44)$$

So, the cell power density at its geometric current density, i_{geom}, is given by

$$\dot{p}_{density} = \left(E_{actual}i_{geom}\right) = \left(E_T - \frac{i_{geom}l_{electrolyte\text{-}separator}}{\sigma_T}\right)\times i_{geom}\ ;\ \left(\frac{(J.s^{-1}) \text{ or } W}{cm^2_{geom}}\right). \quad (45)$$

3. VOLTAGE AND EFFICIENCY RESULTS BASED ON THE CELL FORMULATION

The computed data from the cell formulation presented in Section 2 are presented here. The thermodynamic property data, employed for the computation of the data presented in the tabular form in this section, were taken from Ref. [30]. Numeric data is presented in tabular form in Appendix A.

Figure 2 shows that the cell standard-state voltage,

E_T^o and E_T decrease with an increase in the cell temperature, $T[K]$. Also, at any temperature; E_T^o is larger than E_T for the case, $\left(y_{O_2(g)} = 0.21 \text{ and } \frac{P}{P^o} = 1\right)$. For this case, E_T values are only slightly less than those of E_T^o values; the maximum difference is less than 40 millivolt over the temperature range of 298.15-1100 K. For this reason, the (E_T^ovs.T) plot merges with the ($E_T$vs.T) plot as shown by the red line in Figure 2.

At each temperature,

$E_T\left(\text{for the case, } y_{O_2(g)} = 0.21, \frac{P}{P^o} = 5\right)$ is greater than that for the case $\left(y_{O_2(g)} = 0.21 \text{ and } \frac{P}{P^o} = 1\right)$; however, the difference between them is in the millivolt range.

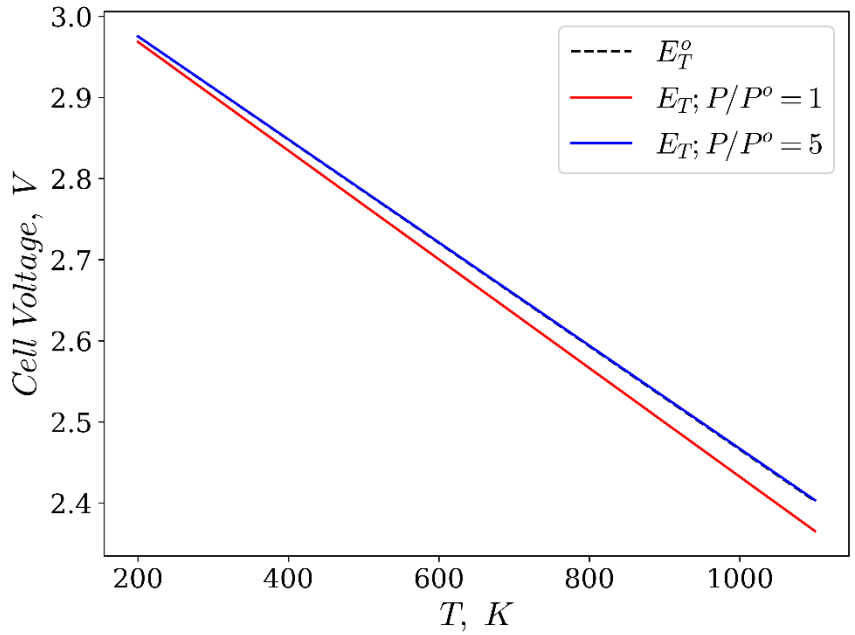

Figure 2. Open-circuit cell voltage versus cell temperature at two oxidant reactant pressures.

Figure 3 shows the cell thermodynamic efficiencies, η_T^o and η_T as a function of the cell temperature,$T[K]$. Both of these decrease with an increase in the cell temperature. The thermodynamic efficiency, η_T^o is greater than η_T for the cases; $(y_{O_2(g)} = 0.21 \text{ and } \frac{P}{Po} = 1 \text{ and } 5)$; the maximum difference being of the order of 1%. Due to the very small difference between the numerical values of η_T^o and η_T(for the case of $y_{O_2(g)}$, $\frac{P}{P^o} = 1$), the (η_T^o vs. T) plot merges with the ($\eta_T$vs. T) plot as shown by the red curve in Figure 3.

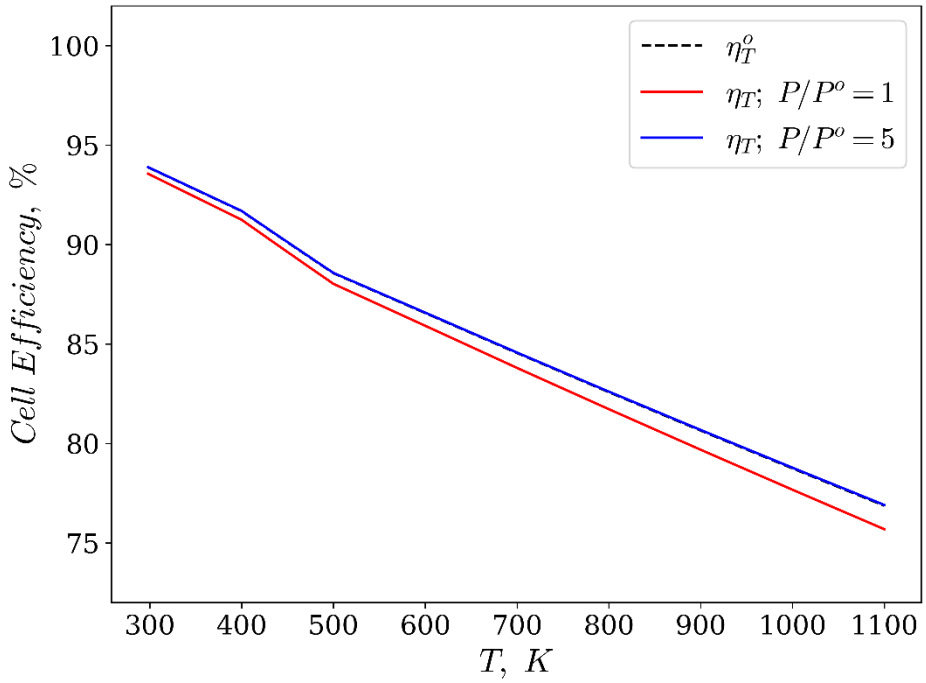

Figure 3. Thermodynamic efficiency of the cell as a function of temperature.

Figure 4 shows that the ratio,

$$\left(\frac{\dot{m}_{(Li+Li_2Q(cr))}}{\dot{P}} = \frac{\left(\text{rate of increase in the cell net weight}\right)}{\text{cell electric power delivery to an external electrical load}} \right)$$ increases as a function of the cell operational temperature over the temperature range: 298.15-1100 K.

Equation (37) shows that this ratio is inversely proportional to the actual cell voltage, E_{actual} (volt) or the cell open-circuit voltage, E_T (volt).

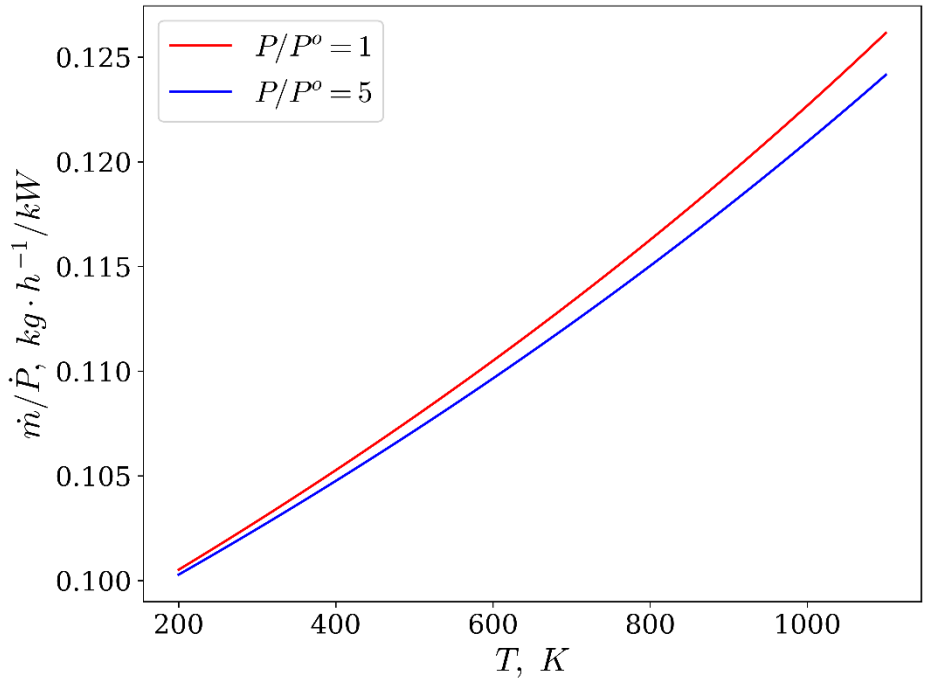

Figure 4. Increase in cell mass per unit of cell electric power delivery as a function of temperature for two different oxidant pressures.

4. CONCLUDING REMARKS

The work reported in this paper is for the performance analysis as well as the design of a cell of the type shown in Figure 1. The cell is to be fed with oxygen continuously either as pure dry oxygen or air; whereas, lithium (fuel) would be fed in the batch-form feed.

(a) The formulation provided in this paper was developed to predict the following:

The cell open-circuit voltage; cell thermodynamic efficiency; lithium-fuel fractional conversion and the formation of the product, $Li_2O(cr)$, as a function of the cell operational time; and the rate of net increase of cell mass (excluding 'free' oxygen) at a constant cell operational current. The formulation also provides the relation to determine the ratio of the cell net mass increase rate to its electric power delivered to an external electric load.

(b) The cell standard-state, E_T^o, and open-circuit, E_T, EMFs (voltages) decrease with an increase in its operational temperature; E_T^o being larger than E_T for the case: $y_{O_2(g)}=0.21$ and $\frac{P}{P^o}=1.$ At each temperature, E_T for the case $\left(y_{O_2(g)}=0.21,\ \frac{P}{P^\circ}=5\right)$ is greater than that for the case $\left(y_{O_2(g)}0.21,\ \frac{P}{P^o}=1\right)$ over the entire temperature range of 298-1100K. The ideal cell thermodynamic efficiency decreases with an increase in the cell temperature. Ratio of (the cell net mass increase rate) to (the cell electric energy delivery rate to an external electric load) increases with an increase in the cell operational temperature; the arithmetic average value of this ratio being:

$$\left[\left(3.3875\times10^{-5}\right)\frac{\left(\text{kg.h}^{-1}\right)\left(\text{kW}\right)^{-1}}{(\text{degree Kelvin})}\right].$$

(c) Finally, it is 'strongly' suggested that an experimental cell system of the type shown in Figure 1 be developed to acquire the actual cell voltage data to validate the predictions of the formulation presented in this paper under the cell isothermal and constant current conditions. Also, the intrinsic electrochemical reaction-rate law of the Butler-Volmer type [32]; especially, for the porous composite cathode, C, of the cell shown in Figure 1 must be developed for its future application for the evaluation of the cell voltage loss due to the occurrence of the electrochemical reaction rate in the cell cathode when the cell is delivering electric power to an external electric load.

Appendix A

Table 1. Numeric data for Figure 2 regarding the open cell voltage.

T, K	E_T^o, V	$E_T, V;\ P/P^o=1$	$E_T, V;\ P/P^o=5$
298.15	2.9128	2.9028	2.9132
300	2.9117	2.9016	2.912
400	2.848	2.8346	2.8484
500	2.7843	2.7675	2.7849
600	2.7207	2.7005	2.7213
700	2.657	2.6335	2.6577
800	2.5934	2.5665	2.5942
900	2.5297	2.4994	2.5306
1000	2.466	2.4324	2.4671
1100	2.4024	2.3654	2.4035

Table 2. Numeric data for Figure 3 regarding the cell thermodynamic efficiency.

T, K	$\eta_T^o, \%$	$\eta_T, \%;\ P/P^o=1$	$\eta_T, \%;\ P/P^o=5$
298.15	93.9	93.6	93.9
300	93.8	93.5	93.9
400	91.7	91.2	91.7
500	88.6	88.0	88.6
600	86.6	85.9	86.6
700	84.5	83.8	84.6
800	82.6	81.7	82.6

900	80.6	79.7	80.7
1000	78.7	77.7	78.8
1100	76.9	75.7	76.9

Table 3. Numeric data for Figure 4 regarding the rate of mass increase per unit electric power output.

T, K	$\dot{m}/\dot{P}, kg/kW;\ P/P^o = 1$	$\dot{m}/\dot{P}, kg/kW;\ P/P^o = 5$
298.15	0.1028	0.1024
300	0.1028	0.1025
400	0.1053	0.1048
500	0.1078	0.1072
600	0.1105	0.1097
700	0.1133	0.1123
800	0.1163	0.115
900	0.1194	0.1179
1000	0.1227	0.121
1100	0.1262	0.1242

REFERENCES

1. J.P. Fellner and S.S. Sandhu. Diffusion-limited Self-Discharge Reaction in the Hubble Space Telescope-Battery. Journal of Power Sources, Vol. 58, pp. 099-102 (1996).
2. J.P. Fellner and S.S. Sandhu. Diffusion-limited Model for a Lithium/Polymer Battery. Electrochimica Acta (The Journal of the International Society of Electrochemistry) Vol. 43, No. 10, 11, pp.1607-1613 (1998).
3. J.P. Fellner, G.J. Loeber, and S.S. Sandhu. Testing of Lithium-Ion-18650 Cells and Characterizing /Predicting Cell Performance. The Journal of Power Sources (The International Journal on the Science and Technology of Electrochemical Systems) Vol. 81-82, pp. 867-871 (1999).
4. S.S. Sandhu and J.P. Fellner. Thermodynamic Equations for a Model Lithium-Ion Cell. Journal of Electrochimica Acta, Vol. 45, No. 6, pp.969-976 (1999).
5. S.S. Sandhu, R.O. Crowther, S.C. Krishnan, and J.P. Fellner. Direct Methanol Polymer Electrolyte Fuel Cell Modeling: Reversible Open-Circuit Voltage and Species Flux Equations. Journal of Electrochimica Acta, Vol. 4, No. 14-16, pp.2295-2303 (2003).
6. S.S. Sandhu, Y.A. Saif, and J.P. Fellner. A reformer performance model for fuel cell applications. Journal of Power Sources, Vol. 140, No.1, pp.88-102 (2005).
7. S.S. Sandhu, R.O. Crowther, and J.P. Fellner. Prediction of Transport Fluxes of Species $\left(H^+, CH_3OH, H_2O\right)$ Through a Solid Polymer Electrolyte Membrane of a Direct Methanol Fuel Cell. Journal of Electrochimica Acta, Vol. 50, pp. 3985-3991 (2005).
8. S.S. Sandhu and J.P. Fellner. Performance/design formulation for a solid polymer-based acid electrolyte hydrogen/air fuel cell. Journal of Power Sources, Vol. 161, No.2, pp. 1133-1153 (2006).
9. S.S. Sandhu, J.P. Fellner, and G.W, Brutchen. Diffusion-limited Model for a Lithium/Air Battery with an Organic Electrolyte. Journal of Power Sources, Vol. 164, pp. 365-371 (2007).
10. S.S. Sandhu, G.W, Brutchen, and J.P. Fellner. Lithium/Air Cell: Preliminary Mathematical Formulation and Analysis. Journal of Power Sources, Vol. 170, pp. 196-209 (2007).
11. S.S. Sandhu and J.P. Fellner. Model Formulation and Simulation of a Solid-State Lithium-Based Cell; featured online, "Renewable Energy Global Innovations". (ISSN 2291-2460). (http://reginnovations.org) August 2013.
12. S.S. Sandhu and J.P. Fellner. Model Formulation and Simulation of a Solid-State lithium-Based Cell. The International Journal of Electrochimica Acta, Vol. 88, pp.496-506 (2013).
13. S.S. Sandhu and J.P. Fellner. Characterization of Iron Phthalocyanine as the Cathode Active Material for Lithium-Ion Batteries. Journal of Chem Eng. Process Technology, 6: 257. DOI: 10.4172/2157-7048.1000; November 23, 2015.
14. S.S. Sandhu, J.P. Fellner, et al. Electrochemical Characterization of the High Charge Capacity of Copper Phthalocyanine for Primary Batteries. IJETMAS (International Journal of Engineering Technology, Management, and Applied Science (ISN: 2349-4476)) Vol. 5, No. 11, pp.24-35, November 2017.
15. S.S. Sandhu, et al. An insightful theoretical model of the performance behavior of a lithium-ion cell electrode. Current Topics in Electrochemistry, Vol. 19, pp.91-103 (2017).
16. S.S. Sandhu, C.J. Cashion, and J.P. Fellner. Modeling and experimental investigations of lithium-

copper phthalocyanine based cells/batteries. RA Journal of Applied Research (ISSN: 2394-6709), Vol. 5, No. 2, pp.2311-2316 (2019). (https://doi.org/10.31142/rajar/v5i2.075)

17. S.S. Sandhu, C.J. Cashion, and J.P. Fellner. Mathematical Model for Lithium-Ion Intercalation into the Cathode Active Material of a Lithium-Based Cell/Battery. RA Journal of Applied Research (ISSN: 2394-6709), Vol. 5, No. 2, pp.2324-2328 (2019). (https://doi.org/10.31142/rajar/v5i2.07)
18. S.S. Sandhu and J.P. Fellner. Ab-initio Calculations for a Lithium/Di-quinoxalinylene Battery. Invention Journal of Research, Technology, in Engineering Management [(IJRTEM), (ISSN: 2455-3689)] Vol.4, Issue 1, pp. 06-10. January-February 2020.
19. S.S. Sandhu and S.T. Kosir. Overall Semi-Empirical Rate-Law Formulation of a Lithium-Based cell or Battery. RA Journal of Applied Research (ISSN: 2394-6709) Vol. 6, No. 08, pp. 2708-2712 (2020).
20. S.S. Sandhu and S.T. Kosir. Rate-Law Application to Simulate Lithium-Based Cell Experimental Data. RA Journal of Applied Research (ISSN: 2394-6709) Vol. 6, No.12, pp.2806-2809 (2020). (https://doi.org/10.47191/rajar/v6i12.06)
21. S.S. Sandhu, S.T. Kosir, and J.P. Fellner. Thermal Energy Production and Heat Exchange between an Electrochemical Cell and Its Surroundings. Ra Journal of Applied Research (ISSN: 2394-6709) Vol. 7, No. 9, pp.2497-2502 (September 2021). (DOI: 10.47191/v7i9.03).
22. S.S. Sandhu, S.T. Kosir, and J.P. Fellner. Thermal Energy Production in an Electrochemical Cell and Heat Transfer to Its Dark Surroundings. RA Journal of Applied Research (ISSN: 2394-6709) Vol. 7, No. 10, pp. 2559-2562 (October 2021). (DOI: 10.47191/rajar/v7i10.05).
23. S.S. Sandhu, J.P. Fellner and P. Chen. On the Diffusion-Controlled Transport and Accumulation of Lithium in an electrode of a Lithium-Based Galvanic Cell. RA Journal of Applied Research (ISSN: 2394-6709) Vol.8, No.1, pp. 41-46 (2022). (DOI: 10.47191/rajar/v8i1.08).
24. S.S. Sandhu. Shrinking Core Model Formulation for the Electrochemical Performance Analysis of a Lithium/Carbon Monofluoride Cell. RA Journal of Applied Research (ISSN: 2394-6079) Vol. 09, No. 04 (March 2023). (DOI: 10.47191/rajar/ v9i4.04).
25. S.S. Sandhu. Formulation for the Performance Analysis of a Lithium-Carbon Monofluoride Cell. RA Journal of Applied Research (ISSN: 2394-6079) Vol.09, No. 04 (April 2023).
26. S.S. Sandhu and K.R. Hinkle. Formulation of an Ideal Solid Oxide Fuel Cell. RA Journal of Applied Research (ISSN: 2394-6709) Vol. 10, No.03, pp.48-52 (March 2024). (DOI: 10.47191/rajar/v10i03.02).
27. S.S. Sandhu and K.R. Hinkle. High Temperature Solid Oxide Electrolyte Fuel Cell Formulation: Non-Steady State Utilization of Fuel and Oxidant. RA Journal of Applied Research (ISSN: 2394-6709) Vol. 10, No. 05, pp.95-102 (May 2024). (DOI: 10.47191/rajar/v10i05.01).
28. A.J. Appleby and F.R. Foulkes. Fuel Cell Handbook; p.588. Van Nostrand Reinhold, New York.
29. M.A. Borik, et al. Structure and conductivity of yttria and Scandia-doped zirconia crystals grown by skull melting. J Am Ceram Soc. 2017; 100:5536-5547. (https://doi.org/10.1111/jace.15074).
30. JANAF Thermochemical Tables (Second Edition), NSRDS-NBS 37. Nat. Stand. Ref. Data Se., Nat. Bur. Stand. (U.S.), 37, 1141 pages (June 1971). CODEN: NSRDA. Issued June 1971.
31. J.M. Smith, H.C. Van Ness, and M.M. Abbot. Introduction to Chemical Engineering Thermodynamics, p.494 (2005, 7th Edition). McGraw Hill Higher Education, Inc.
32. J. Newman and N.P. Balsara. Electrochemical Systems, p. 174. (2021, 4th edition) John Wiley & Sons Inc.